FRP Offshore Structure Connections Optimization and Validation by Classification Society standards

Alfons Borrás[1,2*], Fermín Otero[1,2] and Xavier Martínez[1,2]

[1] International Center for Numerical Methods in Engineering (CIMNE), Universidad Politécnica de Cataluña, Campus Norte UPC, 08034 Barcelona, Spain, e-mail: cimne@cimne.upc.edu, web page: http://www.cimne.com/

[2] Barcelona School of Nautical Studies, Universitat Politècnica de Catalunya, Pla de palau, 18, 08003 Barcelona, Spain, e-mail: info@fnb.upc.edu - Web page: http://www.fnb.upc.edu/

[*] Corresponding author: Alfons Borrás, alborras@cimne.upc.edu

ABSTRACT

This paper discusses the use of composite materials in the design process of a horizontal bracing to column connection of an offshore semi-submersible platform to support two wind turbines. The geometry of the connection was optimized to improve the performance and reliability of the connection, columns and bracing tubes.

These offshore foundations usually deal with massive structural tubes, and they are used to fit a huge amount of stiffeners. This paper will show how using some horizontal stiffeners combined with their intersection with horizontal bracings tubes, can improve drastically the behavior of the connection. A comparison between conventional materials (steel) and advanced materials (E-glass fibres and epoxy matrix) was performed and it was demonstrated how the use of composite materials makes necessary to modify the connection geometry and configuration to obtain an equivalent performance. This is due to the very different stiffness behavior shown by composites and steel. Therefore, the design of an offshore connection must be approached differently according to the used material.

The composite laminate layout design process was also made. The material was evaluated using a Bureau Veritas normative note specifically applicable to composite ship hulls, but adapted to the needs of the materials used in this design, in terms of raw material requirements. The design process of a laminate panel of the connection is shown using the above mentioned standard.

All data and results shown here were harvested within the scope of the European research project Fibregy (EU Horizon 2020, Ref. 952966).

Keywords: Composite Materials; Offshore Floating Platforms; Connections; Fibregy.

NOMENCLATURE

ρ	Density of an individual layer (g/cm^3)
ρ_r	Resin density (g/cm^3)
ρ_f	fiber density (g/cm^3)
V_f	Volume fraction of the reinforcements ($parts \quad per \quad unit$)
M_f	Mass fraction content of the reinforcements ($parts \quad per \quad unit$)
e	Layer thickness (mm)
P_f	Total mass per square meter of dry reinforcement fabric in (g/m^2)
E_{UDi}	Elastic Young modulus of the layer in specified direction (MPa)
G_{UDi}	Shear modulus of the layer in specified direction (MPa)
ν_{UDij}	Poisson coefficient of the layer in specified direction
E_{f_i}	Fibre Young modulus in specified direction (MPa)
E_r	Matrix Young modulus (MPa)
G_f	Shear modulus of the fibre (MPa)
G_r	Shear modulus of the resin (MPa)
E_i	Main tensile modulus of the laminate in specified global direction (MPa)
G_{xy}	laminate in-plane shear modulus (MPa)
ν_i	Poisson coefficient in specified laminate axis
V_i	Laminate neutral axis location in specified axis position (mm)
$[EI]_i$	Laminate bending rigidity, specified global axis ($N.mm^2$)
th	Laminate thickness (mm)
Z_i	Distance between the edge of the laminate and the mid-thickness of each layer (mm)
ε_i^0	Tensile or compression strain of the laminate median plane in specified direction (MPa)
γ_{xy}^0	Shear strain of the laminate median plane in XY plane (MPa)
K_i	Curved deformation of the laminate median plane around specified axis
ε_i	Strains of each individual layer, calculated at its mid-thickness in the laminate global axes
ε_n	Strains of each individual layer, calculated at its mid-thickness in its own local axes
σ_i,τ_{ij}	Stresses in an individual layer expressed in its own local axes (MPa)
σ_{br}, τ_{br}	Theoretical breaking stresses of a layer (MPa)

1. INTRODUCTION

In order to reach Paris Agreement goals, it seems unavoidable to quit using fossil fuels to reduce emissions of greenhouse gases. In this context the generation of energy will have an increasingly renewable source, and wind power generation is expected to play a major role in the near future. Due to related drawbacks on onshore wind power generation, such every time fewer available locations, less wind power specific energy than offshore, higher turbulence, higher wind shear, and generation of social conflicts (Oh et al. 2018), offshore wind generation will increase its presence across. Specifically in Europe, it will increase its contribution around 60 or 70 times by 2030 compared to its installed capacity in 2020 (González and Diaz-Casas 2016).

So far, most offshore wind farms are installed in water depths below 50 meters, using so-called fixed foundations to the bottom. If depth is less than 30 meters, usually large diameter steel monopiles or gravity bases are used, and from 30 meter-deep to 50 meter-deep, jacket or tripod structures are the chosen option (Manzano-Agugliaro et al. 2020). However, to harvest the highest available energy it is needed to operate in deeper waters, and in addition to this, many countries feature continental shelf configuration that drops suddenly, making installation of fixed structures much more difficult.

Thinking about waters deeper than 50 meters, floating structures formerly used in the oil and gas industry, for example, TLP's, SPAR's and semi-submersible are being studied the most to be adapted to wind energy field. This structures have been traditionally built using steel, but new materials are being studied to be adapted to this kind of structures as well. Composite materials to be applied may be a reliable option due to their low weight, resistance to water sea, and consequently minimizing corrosion issue, and good behavior against fatigue (Jurado Granados 2021).

In this context, the Fibergy project was born with the objective of demonstrating the feasibility of building a semi-submersible foundation for wind turbines made of composite materials, studying the design, manufacturing and assembly processes, and starting from the steel-based design of the former W2Power platform (Fig. 1).

Figure 1: W2Power steel platform

(**Enerocean**)

The design process of such large structure, based on composite materials faces a lot of challenges, and connections between tubes could be considered a hot spot to be accurately assessed. The lack of regulations to assist the design process makes the task harder. So, the geometry optimization process of a connection will be shown here. The design process will be backed using a Bureau Veritas guide note related to composite hulls design when needed.

2. PLATFORM AND CONNECTION OVERVIEW

The W2Power concept (Fig. 2) is a three-legged foundation and it takes advantage of its 9 meter-diameter each 3 hollow columns to provide necessary buoyancy. Horizontal 2.8 meter-diameter ring bracing tubes connecting columns and extra tubes are added to increase the integrity and total stiffness of the structure. A footplate is added to the base of each column to provide additional hydrodynamic inertia to the foundation. Two columns are used to support one wind turbines each.

To achieve an economically balanced and viable foundation, carbon fiber reinforcement (CFRP) was to be used for both towers and glass fiber reinforcement (GFRP) for the rest of the structure. The design of the towers with CFRP was also another milestone of the project, as there has not been much research on composite wind turbine towers, where steel was still massively used.

The main objective of this paper is to evaluate the connection between the columns and the horizontal bracing tubes of the structure, since it is expected that due to the combined wave and sea loads, this point may be highly stressed, so it must be accurately analyzed.

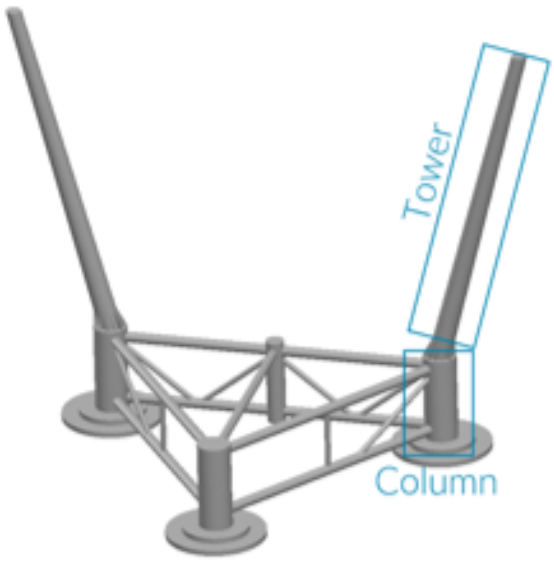

Figure 2: W2Power concept

(**Fibregy**)

3. CONNECTION OPTIMIZATION

Quite a few large offshore tubular steel structures have been built for the oil and gas industry for years, and this trend has also been extended to offshore wind turbine foundation structures. Thus, it is not surprising to say that most of the designs introduced have been developed using tubular tubes and their joints have been made joining tube to tube, and in most cases, welded, due to their efficiency and reliability (Marshall 2013), although bolted joints are under study to know their benefits and efficiency (Mehmanparast, Lotfian, and Vipin 2020). Tubular structures have been highly appreciated for years for their better behavior against drag forces, but other factors must be taken into account, mainly because new materials are being introduced for their use.

Therefore, in recent years, new studies have been conducted to explore other alternatives to traditional round tubular connections. For example, Fig. 3 shows a square-shaped multiple connection, while other approaches aim to design the entire structure using square-shaped profiles. Fig. 4 illustrates the VolturnUS floating foundation structure developed by the Center for Advanced Composite Structures and Materials at the University of Maine.

The Fibregy project has also been working on the optimization of the connections to check which would be the best option, from the point of view of feasibility and also adapted to new materials.

3.1 Connection preliminary design

The first design tried to reply the original W2Power concept. This is, tubular structures without any kind of transition.

Fig. 5 illustrates the connection of the bracing (red-coloured tube) to the column (blue-coloured tube) in its original design, without stiffeners nor other structural elements, except for the reinforcing flange (purple-coloured flange). Note that this is a massive structure in which the column is a 9-meter diameter tube, and the horizontal bracing is a 2.8-meter diameter tube. Steel-based thicknesses were

Figure 3: Multiple square-shaped connection

(**Fibergy**)

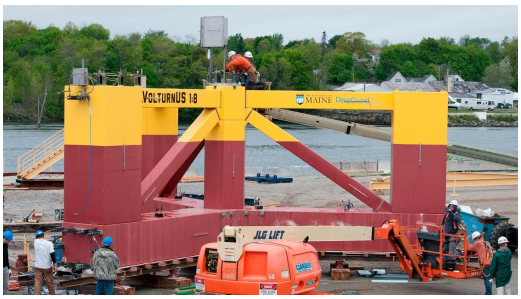

Figure 4: VolturnUS floating offshore foundation. Maine University

(**Maine University**)

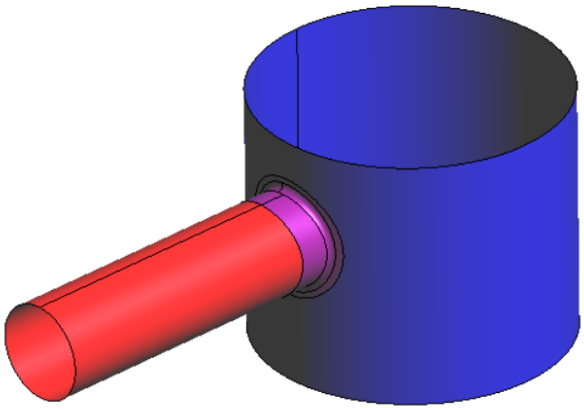

Figure 5: Connection original design

considered as a result of previous tests corresponding to 16 mm for the column, 28 mm for the bracing and 28 mm for the connecting flange.

3.2 Simulation Loads

A floating foundation has to bear different loads, whether from tower, nacelle and blade loads, aerodynamic forces and wave loads. Wave loads are usually calculated taking into account the localization where the offshore structure is going to be installed, and an extreme sea state would be calculated and a seakeeping analysis would be carried out. However, eventually it was considered to load the connection with massive bending forces in order to asses its behaviour and how this stress distribution was being improved as long as the geometry was being optimized. Therefore, the same force was applied to all cases studied here, in order get a proper comparison between them, with reasonable strengths and stresses, rather than obtaining quantitative values. This force consists on a vertical displacement at the end of the bracing that creates a bending moment at the connection. The reason behind the selection of this load is that this is one of the most demanding load scenarios for this connection.

3.3 Geometry optimization

First simulations tried to optimize round-shaped tube connections, all of them fitting a reinforcement flange (purple element in Fig. 5), but with different ending configurations. The reinforcement flange was considered as bonded. Some configurations had tubes that went through into the column and other don't, then first differences were found out. Then the shape of the tube was modified when joining to the column to get a better response. Some frames were implemented to obtain much better performance as well. Optimization process was carried out using isotropic material (steel) in order to minimize the computational cost and to avoid affecting the solution by the orthotropy provided by composite materials. Once the optimal shape was reached, laminate material was introduced to check the joint behavior.

3.3.1 Round-shaped tube joints

The first connections considered were round-shaped. The first one consisted in the plain intersection of the tube to the column without any frame nor stiffener (Fig. 6). In the second connection considered two horizontal stiffeners are added in the column to facilitate the transmission of stresses (Fig. 7). Finally a third connection was considered that reinforced the configuration of the previous connection (Fig. 8) with a bracing tube passing through the column until its middle axis.

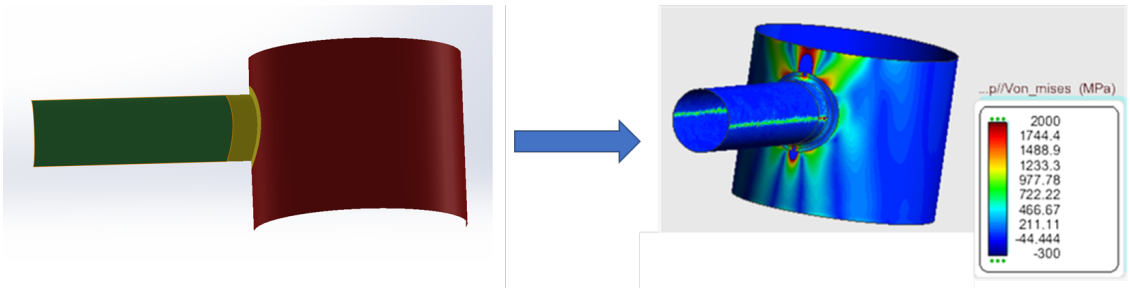

Figure 6: Round-shaped joint, intersected column, without horizontal stiffeners

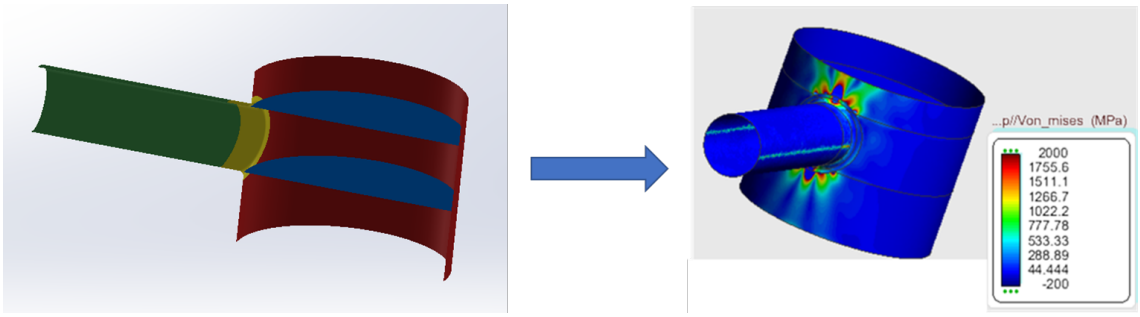

Figure 7: Round-shaped joint, intersected column, with two horizontal stiffeners

It was quickly observed that the intersection with the column wall performed unacceptable stresses values around the surrounding areas of the flange and along the column section, while the rest of the material was under acceptable conditions (Fig. 6). This effect was reduced with the second connection considered, adding two horizontal stiffeners (Fig. 7). However, although some stress reduction was achieved, the the final stresses are still too far from the desirable values. Among other reasons, these

excessive stresses can be explained by the fact that these two horizontal stiffeners were not in contact with the horizontal bracing tube, as it does not pass through the column.

To take advantage of the horizontal stiffeners, the third connection forced the tube to into the column up to half its diameter. In this last case both stiffeners were attached to the tube inside the column (Fig. 8).

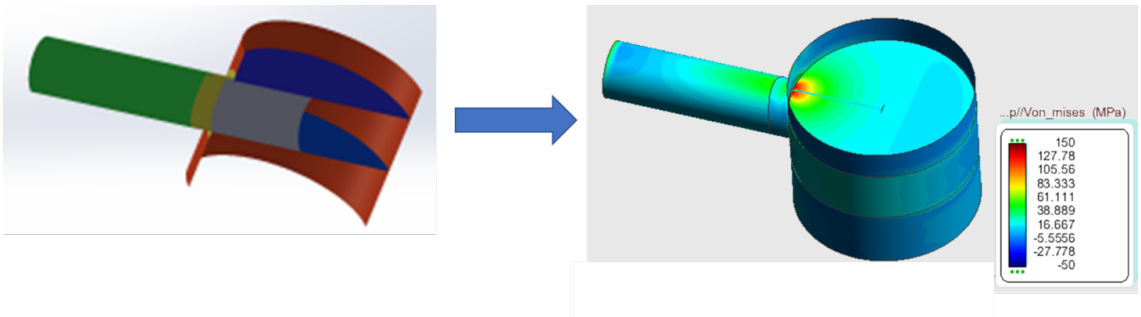

Figure 8: Round-shaped joint with tube attached to two decks

Although it was checked that the addition of two horizontal stiffeners improved significantly the performance of the connection as stresses dropped off dramatically and the behavior of all elements of the joint were relatively uniform, there still was a zone with higher stress concentration on the horizontal stiffeners next to the column (Fig. 8, right). It could be a consequence of the circular shape of the bracing, so, it made sense to develop squared transitions into the column to increase the surface area in contact between horizontal stiffeners and bracing tube.

3.3.2 Square-shaped tube joints

To avoid all problems featured by round-shaped joints, the circular section of the horizontal bracing was modified to square-shaped section, with a smooth transition, when it reached the connection. Stresses and deformations were highly reduced compared to prior models just around the connection point. Connection between tube and column was completely smooth with lower stress values compared to prior designs. In order to improve the performance of the connection, a 500 millimeter-radius rounded chamfer was implemented and optimized to obtain even a smoother transition between tube and column.

A third horizontal stiffener was fitted halfway up the horizontal bracing. It was done this way because using squared tubes instead of circular tubes may feature some buckling issues. This article will not consider holes and stiffeners that would be required for horizontal stiffeners to avoid problems of denting and column cutouts.

4. MATERIAL SELECTION

4.1 Composite layer design

There is no general agreement on which would be the most suitable material to apply to an offshore foundation, carbon fiber or fiberglass. So, in the framework of Fibregy project, different multi-criteria matrices were created to select the material, weighing the technical, economic and environmental properties, and finally the final material was characterized:

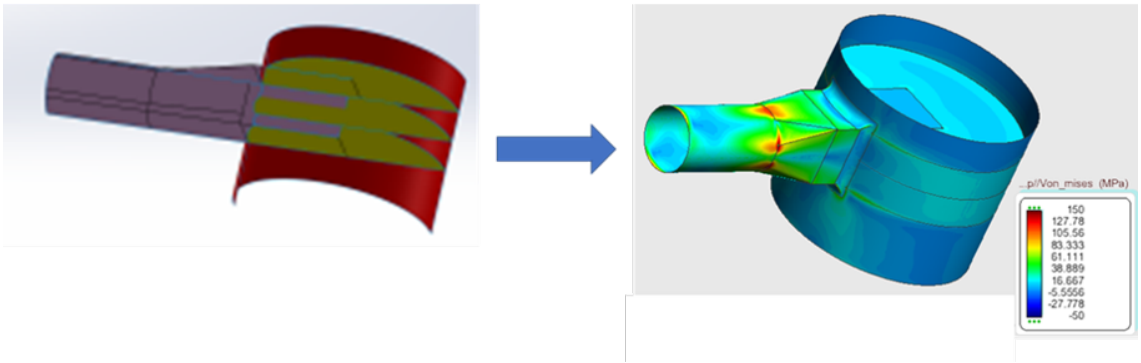

Figure 9: Squared-shape joint with tube attached to two horizontal stiffeners and an intermediate horizontal stiffener

- Fibres: Unidirectional Saertex E-Glass fabric (material no 30007627). Areal density: 1182 g/m^2.
- Matrix: Infugreen 810, two-component epoxy system.

As said before, due to the innovative nature of the Fibregy project, it is not surprising the lack of standards or guidelines that could define the steps to carry out this assessment process. Specifically, no specific standard or guideline for the assessment of the structure of an offshore floating foundation made with FRP material, issued by any Classification Society (SSCC) or other international institution, has been found. However, for evaluating the performance of laminates, Bureau Veritas NR 546 DT R03 (November 2018) has been used to do all needed ply and laminate calculations.

According to this Bureau Veritas Rule note, density of an individual layer can be obtained from:

$$\rho = \rho_f V_f + \rho_r (1 - V_f). \tag{1}$$

Being V_f:

$$V_f = \frac{M_f/\rho_f}{M_f/\rho_f + (1 - M_f)/\rho_r} \tag{2}$$

Concerning the individual layer thickness, it may be calculated according to the following expression:

$$e = \frac{P_f \left(\frac{1}{\rho_f} + \frac{1-M_f}{M_f \rho_r}\right)}{1000} \tag{3}$$

The longitudinal elastic Young modulus of the ply E_{UD1} is estimated by the following expression:

$$E_{UD1} = C_{UD1} \left(E_{f_0} V_f + E_r (1 - V_f)\right), \tag{4}$$

The transverse Young moduli E_{UD2} and E_{UD3} can be found using:

$$E_{UD2} = E_{UD3} = C_{UD2} \left[\left(\frac{E_r}{1 - \nu_r^2} \right) \frac{1 + 0.85 V_f^2}{(1 - V_f)^{1.25} + \frac{E_r}{E_{f_{90}}} \frac{V_f}{1 - \nu_r^2}} \right], \tag{5}$$

Shear moduli G_{UD12}, G_{UD13} and G_{UD23} are obtained applying:

$$G_{UD12} = G_{UD13} = C_{UD12}\, G_r\, \frac{1 + \eta V_f}{1 - \eta V_f} \quad ; \quad G_{UD23} = 0.7\, G_{UD12} \tag{6}$$

with,

$$\eta = \frac{\left(\frac{G_f}{G_r}\right) - 1}{\left(\frac{G_f}{G_r}\right) + 1}, \tag{7}$$

To calculate Poisson coefficients ν from volume fraction of fibers and resin:

$$\nu_{UD13} = \nu_{UD12} = C_{UDV}\left[\nu_f V_f + \nu_r(1 - V_f)\right] \quad ; \quad \nu_{UD21} = \nu_{UD31} = \nu_{UD12}\frac{E_{UD2}}{E_{UD1}} \tag{8}$$

Take note that C_{UD1}, C_{UD2}, C_{UD12}, and C_{UDV} are Bureau Veritas experimental coefficients with values of 1, 0.8, 0.8, and 0.9 respectively for E-Glass Fibres.

All layers were considered to feature Uni Directional fiber configuration (UD), and fiber mass content was considered to be 65%. Physical characteristics and elastic properties of a layer are shown in Table 1 and Table 2 respectively.

$Mass/m^2$ of Fibre (g/m^2)	$Mass/m^2$ of Resin (g/m^2)	$Mass/m^2$ of Ply (g/m^2)
1182	636	1818

Ply thickness (mm)	Areal ply density (g/cm^3)
0,969	1,876

Table 1: Layer main physical characteristics

E_1 (MPa)	E_2 (MPa)	G_{12} (MPa)	G_{13} (MPa)	G_{23} (MPa)	ν_{12}	ν_{21}
36231	7398	3382	3382	2367	0.286	0.058

Table 2: Layer main elastic properties

4.2 Laminate configuration

Since composites allow different materials and layouts to be combined, there is the possibility of achieving a nearly infinite number of combinations for a given problem. This flexibility also implies the need to design specific composite materials for different parts of the structure, but this approach must take into account the loads applied to the material in order to obtain an efficient solution. In this section it will be shown how the laminate layout of one panel of the horizontal bracing of the bracing (Fig. 10, panel A) can be calculated using Bureau Veritas formulation. This procedure should be repeated for the rest of elements of the structure.

No matter how the final laminate layout is as long as it takes into account EUROCOMP (Clarke 2003) design code minimum requirements. It has been taken into account when designing laminates that at least 12,5% of unidirectional layers must oriented to 90^o, 12,5% oriented to 45^o, and 12,5% oriented to -45%. The rest must be oriented to 0^o. In order to fulfill EUROCOMP requirements, and since it is desired to use symmetric and balanced layouts as well, the design process was based on this configuration: 0^o, 45^o, 0^o, -45^o, 0^o, 90^o and 90^o, 0^o, -45^o, 0^o, 45^o, 0^o. Then, number of layers must be determined. To do so, Bureau Veritas calculation method was carried out.

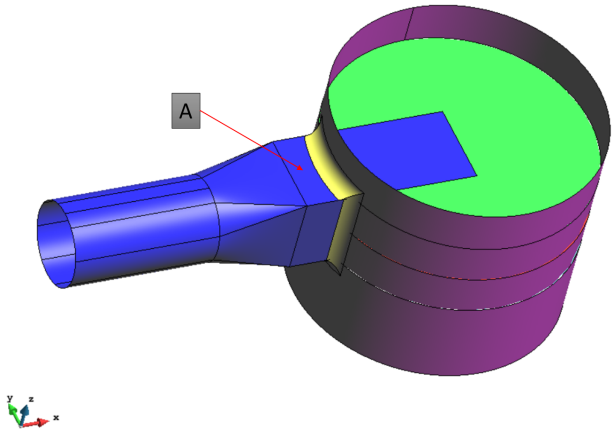

Figure 10: Tested panel

4.2.1 Stresses of individual layers in their own local axes

Since strengths were determined, strains and curved deformations of the laminate may be obtained from the following expression:

$$\begin{bmatrix} \varepsilon_x^0 \\ \varepsilon_y^0 \\ \gamma_{xy}^0 \\ K_x \\ K_y \\ K_{xy} \end{bmatrix} = \begin{bmatrix} A & B \\ B & D \end{bmatrix}^{-1} \begin{bmatrix} N_x \\ N_y \\ N_{xy} \\ M_x \\ M_y \\ M_{xy} \end{bmatrix} \tag{9}$$

Where A, B and D set up the global rigidity matrix ABD.

As will be seen below, two laminate configurations were selected for evaluation, along with the original steel configuration. N_x, N_y, M_x, and M_y forces were determined according to the applied load, and for each material configuration. No relevant differences were found among the three configurations. These values are picked up as seen in Fig. 11, and shown in table 3.

N_x (N/m)	N_y (N/m)	M_x (N/m)	M_y (N/m)
$3.9 * 10^6$	$1.1 * 10^6$	$-5.3 * 10^3$	$-1,6 * 10^4$

Table 3: Determined strengths

Strains of individual layers in the laminate global axes: The in-plane strains ε_x , ε_y and γ_{xy} of each individual layer, calculated at its mid-thickness in the laminate global axes, are given by:

$$\begin{bmatrix} \varepsilon_x \\ \varepsilon_y \\ \gamma_{xy} \end{bmatrix}_k = \begin{bmatrix} \varepsilon_x^0 \\ \varepsilon_y^0 \\ \gamma_{xy}^0 \end{bmatrix} + \begin{bmatrix} K_x \\ K_y \\ K_{xy} \end{bmatrix} * \frac{Z_k + Z_{k-1}}{2} \tag{10}$$

With:

$$Z_k = \frac{-th}{2} + \sum_1^k e_i \quad ; \quad Z_{k-1} = \frac{-th}{2} + \sum_1^{k-1} e_i \tag{11}$$

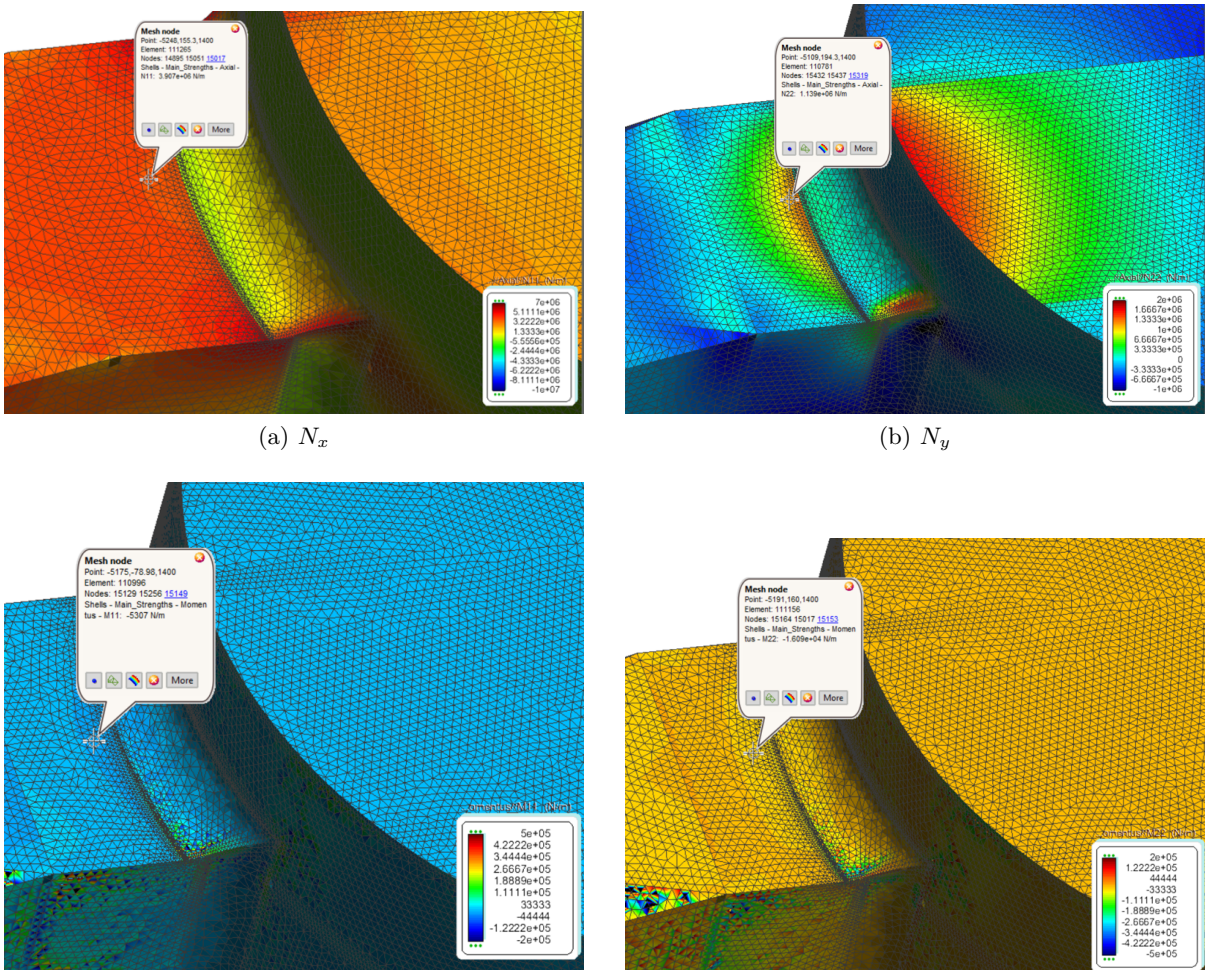

(a) N_x (b) N_y

(c) M_x (d) M_y

Figure 11: Strengths at point A

Strains and stresses of individual layers in their own local axes: The in-plane strains ε_1, ε_2 and γ_{12} of each individual layer, calculated at its mid-thickness in its own local axes, are given by:

$$\begin{bmatrix} \varepsilon_1 \\ \varepsilon_2 \\ \gamma_{12} \end{bmatrix}_k = T'^{-1} \begin{bmatrix} \varepsilon_x \\ \varepsilon_y \\ \gamma_{xy} \end{bmatrix}_k \tag{12}$$

Where T' is the transposed rotation matrix.

Whereas the local stresses σ_1, σ_2 and τ_{12} in an individual layer expressed in its own local axes, at mid-thickness, are defined by:

$$\begin{bmatrix} \sigma_1 \\ \sigma_2 \\ \tau_{12} \end{bmatrix}_k = \left[\bar{R}\right] \begin{bmatrix} \varepsilon_1 \\ \varepsilon_2 \\ \gamma_{12} \end{bmatrix}_k \tag{13}$$

Being $\bar{R}$ local matrix of rigidity.

4.2.2 In-plane theoretical individual layer breaking stresses formulae

Theoretical breaking stresses come out from:

$$\begin{aligned} \sigma_{brt1} = \varepsilon_{brt1} * E_{UD1} * Coef_{res} \quad ; \quad \sigma_{brc1} = \varepsilon_{brc1} * E_{UD1} * Coef_{res} \\ \sigma_{brt2} = \varepsilon_{brt2} * E_{UD2} * Coef_{res} \quad ; \quad \sigma_{brc2} = \varepsilon_{brc2} * E_{UD2} * Coef_{res} \\ \tau_{br12} = \gamma_{br12} * G_{UD12} * Coef_{res} \quad ; \quad \tau_{brIL1} = \gamma_{brIL1} * G_{UD23} * Coef_{res} \\ \tau_{brIL2} = \gamma_{brIL2} * G_{UD13} * Coef_{res} \end{aligned} \tag{14}$$

Where $Coef_{res}$ is a coefficient that takes into account the adhesive quality of the resin system and it has a value of 1.0 when the matrix is epoxy based. Maximum strain values proposed by BV can be used if they are not known. For Unidirectional reinforcements and E-Glass fibres, these are:

ε_{brt1}	ε_{brt2}	ε_{brc1}	ε_{brc2}	$\gamma_{br_{12}}$	$\gamma_{br_{13}}$, γ_{brIL2}	$\gamma_{br_{23}}$, γ_{brIL1}
2.70	0.53	1.80	1.55	1.80	1.80	2.50

Table 4: Bureau Veritas theoretical maximum strain coefficients for E-Glass UD fabrics

4.2.3 Failure Criteria

Main Stresses Analysis in Each Layer: Maximum stresses in each layer of the panel laminate induced by in-plane forces due to global loads must satisfy the following criteria:

$$\sigma \leq \sigma_{br}/S_F \quad ; \quad \tau \leq \tau_{br}/S_F \tag{15}$$

In case of main stresses analysis, safety factor SF must fulfill:

$$S_F \geq C_V * C_F * C_R * C_i \tag{16}$$

Combined Stress Analysis: According to Bureau Veritas regulation, combined stress analysis must be done according to Hoffman criterion. The minimum rule safety factor SF_{CS} is to fulfil the following condition:

$$SF_{CS} > SF_{CSiapp} \tag{17}$$

where:

$$SF_{CS} = C_{CS} * C_V * C_F * C_i \tag{18}$$

And SF_{CSiapp} is equal to the positive value of:

$$SF_{Ciapp} = \frac{-b \pm \sqrt{b^2 + 4a}}{2a} \tag{19}$$

Taking into account:

$$a = \frac{\sigma_1^2}{|\sigma_{brc1}\sigma_{brt1}|} + \frac{\sigma_2^2}{|\sigma_{brc2}\sigma_{brt2}|} - \frac{\sigma_1\sigma_2}{|\sigma_{brc1}\sigma_{brt1}|} + \frac{\tau_{12}^2}{\tau_{br12}^2} \tag{20}$$

$$b = \frac{\sigma_1(|\sigma_{brc1}| - |\sigma_{brt1}|)}{|\sigma_{brc1}\sigma_{brt1}|} + \frac{\sigma_2(|\sigma_{brc1}| - |\sigma_{brt1}|)}{|\sigma_{brc2}\sigma_{brt2}|} \tag{21}$$

Partial Safety Factors: The partial safety factors to be applied are:

- C_V : Rule partial safety factor taking into account the ageing effect on the laminates = 1.2 for monolithic laminates.
- C_F : Rule partial safety factor taking into account the fabrication process and the reproducibility of the fabrication = 1.25 in case of hand lay-up process and strip planking.
- C_R : Rule partial safety factor taking into account reinforcement fabric of the layers = 2.1 for tensile or compressive stress parallel to the continuous fibre, or 1.25 for tensile or compressive stress perpendicular to the fibre.
- C_{CS} : Rule partial safety factor for combined stresses = 1.7 for unidirectional fabric.
- C_i : Rule partial safety factor taking into account the type of loads (sea pressure, dynamic sea pressure or internal pressure). It does not apply.

4.2.4 Layout proposal

Following laminate configuration (Table 5) fulfills failure criteria according to applied loads :

quantity of groups	rotation angle
7	0, 45, 0, -45, 0, 90
7	90, 0, -45, 0, 45, 0

Table 5: Laminate lay-out. Thickness ratio 1:3

It is 84-layer laminate. It was checked how this laminate was far from breaking. Layers 6 and 12 were the most loaded layers. Stress analysis results are shown in table 6.

σ_1 (MPa)			σ_2 (MPa)			τ_{12} (MPa)			Combined Stresses
σ_1	σ_{brt1}	*Ratio*	σ_2	σ_{brt2}	*Ratio*	τ_{12}	τ_{brt12}	*Ratio*	*Ratio*
50.8	981	0.05	16.7	39.2	0.43	–	60.9	–	0.41

Table 6: Layer 6 stress failure analysis. Laminate 1:3 thickness ratio

Main characteristics of the laminate can be calculated as well. The main tensile moduli of a laminate, E_X and E_Y in their main directions can be calculated respectively following:

$$E_X = \frac{1}{A'_{11}\, th} \quad ; \quad E_Y = \frac{1}{A'_{22}\, th} \tag{22}$$

Whereas the in-plane shear modulus G_{XY} of the laminate can be obtained from:

$$G_{XY} = \frac{1}{A'_{33}\, th} \tag{23}$$

Concerning Poisson ratios in their main directions, they can be got from:

$$\nu_X = \frac{A_{21}}{A_{22}} \quad ; \quad \nu_Y = \frac{A_{12}}{A_{11}} \tag{24}$$

The distances V_X and V_Y, between the global neutral axis of a laminate and the edge of its individual layer, are defined in its two main direction by:

$$V_X = \frac{\sum E_{Xi} e_i Z_i}{\sum E_{Xi} e_i} \quad ; \quad V_Y = \frac{\sum E_{Yi} e_i Z_i}{\sum E_{Yi} e_i} \tag{25}$$

The global bending rigidity of a laminate can be expressed, in its two main directions X and Y, following:

$$\left[EI\right]_X = \frac{1}{D'_{11}} \quad ; \quad \left[EI\right]_Y = \frac{1}{D'_{22}} \tag{26}$$

It is worth to say that A_{ij}, A'_{ij}, and D'_{ij} are elements of the global rigidity matrix ABD and reverse global rigidity matrix ABD'.

Laminate characteristics are shown in table 7. Its thickness is 81.40 mm, what is around three times thicker than steel configuration.

Thickness (mm)	Weight (kg/m^2)	Fiber Weight (kg/m^2)
81,40	152,751	99,288
Resin Weight (kg/m^2)	Ex (MPa)	Ey (MPa)
53,462	23.649	14.342
Gxy (MPa)	ν_x	ν_y
5.601	0,289	0,175
Vx (mm)	Vy (mm)	$[EI]_x$ ($N.mm^2$)
40,702	40,702	1,085E9
$[EI]_y$ ($N.mm^2$)	Density (g/cm^3)	
6,101E8	1,876	

Table 7: Laminate global results. Thickness ratio 1:3

4.3 Stiffness analysis

A stiffness analysis was done to asses the behavior of the designed laminate versus steel. It is well known than E-Glass fibres may have some stiffness drawbacks, so, another laminate that doubles thickness of the first one was designed to be included in the analysis (table 8 and table 9).

quantity of groups	rotation angle
14	0, 45, 0, -45, 0, 90
14	90, 0, -45, 0, 45, 0

Table 8: Laminate lay-out. Thickness ratio 1:6

Concerning stresses, this laminate features failure ratios even lower than laminate with thickness ratio 1:3 (table 10).

Displacements of point A of the studied panel were measured in X axis and Z axis. Fig. 12 and Fig. 13 illustrate how the measurements were made, and table 11 shows the ΔX and ΔZ displacements on the basis of steel displacements.

Thickness (mm)	Weight (kg/m^2)	Fiber Weight (kg/m^2)
161,82	303,580	197,327
Resin Weight (kg/m^2)	Ex (MPa)	Ey (MPa)
106.253	23.683	14.188
Gxy (MPa)	ν_x	ν_y
5.608	0,292	0,175
Vx (mm)	Vy (mm)	$[EI]_x$ ($N.mm^2/mm$)
80,912	80,912	8,423E9
$[EI]_y$ ($N.mm^2/mm$)	Density (g/cm^3)	
4,919E9	1,876	

Table 9: Laminate global results. Thickness ratio 1:6

σ_1 (MPa)			σ_2 (MPa)			τ_{12} (MPa)			Combined Stresses
σ_1	σ_{brt1}	*Ratio*	σ_2	σ_{brt2}	*Ratio*	τ_{12}	τ_{brt12}	*Ratio*	*Ratio*
17.6	981	0.02	7.92	39.2	0.20	–	60.9	–	0.13

Table 10: Layer 6 stress failure analysis. Laminate 1:3 thickness ratio

	Laminate 1:3	Laminate 1:6
ΔX displacement (%)	262	60
ΔZ displacement (%)	151	21

Table 11: ΔX and ΔZ displacements laminate configuration 1:3 and 1:6 versus steel

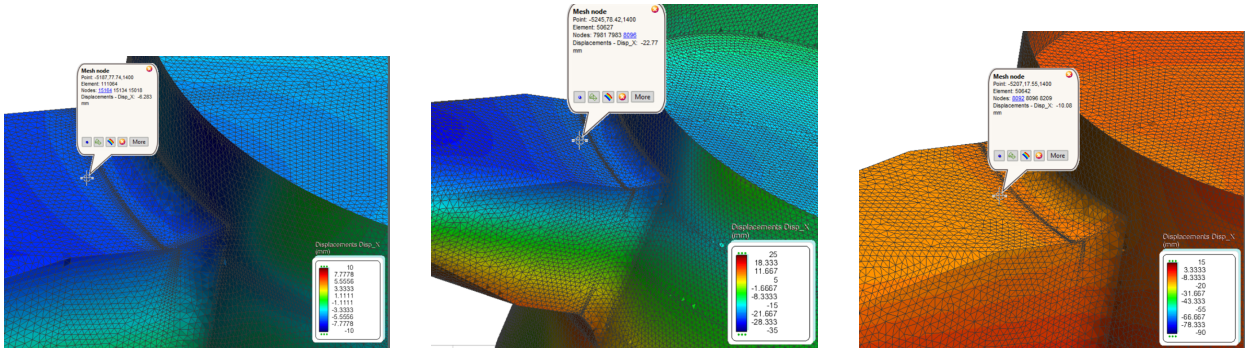

Figure 12: Displacements in X. Steel (left), composite 1:3 (center), composite 1:6 (right)

It can be observed in Table 11 how laminate with thickness relation 1:6 against steel offers more convenient displacement values, but still higher than steel. However, it does not seem reasonable to deal with these kind of massive thicknesses, what leads to state that stiffness is the weak point of this kind of composite structures instead of stresses. While the stress safety factor has been doubled, the displacement is still larger than steel. Bearing in mind that structure stiffness is the cumber-stone of these structures, more efficient solutions, compared to increasing the thickness should be thought. A possible solution should be fitting stiffeners.

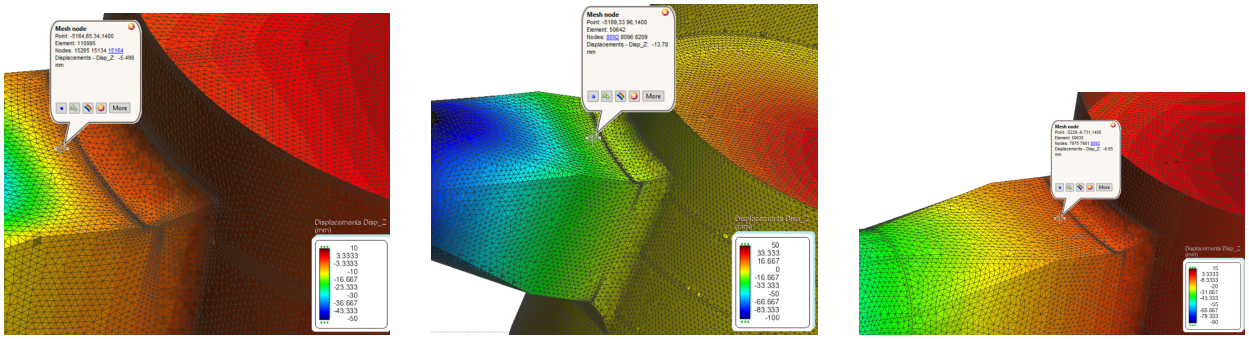

Figure 13: Displacements in Z. Steel (left), composite 1:3 (center), composite 1:6 (right)

5. CONCLUSIONS

Fibregy project has proved the feasibility of manufacturing an offshore floating structure to stand two wind turbines, entirely made of composite material. However, connections between tubes were a hot-spot to be accurately analyzed. A connection between horizontal bracing tube and column has been optimized stating how the use of square transitions and some horizontal stiffeners plates attached to bracing tube can easily decrease stress concentrations. This geometry is also truly useful due to laminate manufacturing process, completely different from usual procedures used dealing with steel.

Although using composites offers some advantages against steel, for instance, it features better resistance of the material against harsh marine environment, better fatigue performance and weight reduction, the design of the structure must be more elaborated. Since composite laminate performance is lower from the point of view of stiffness, it should be necessary to design a complex structure with several stiffeners, which may compromise weight reduction and economic viability of the project if final design is not optimal. Stress problems are not, from the outset, as relevant problems as stiffness problems, since it has been seen that for deformations that could no longer be considered admissible, the stress values were still far from their critical levels.

The lack of specific regulations of classification societies concerning offshore structures made of composite materials was a challenge along the design process of the structure. Bureau Veritas NR 546 was checked and it offered valuable formulation to assess a structure like this one.

6. ACKNOWLEDGEMENTS

The authors would also like to thank all Fibregy consortium for their generous support for this research. This project has received funding from European Union's Horizon 2020 programme under grant agreement ID: 952966. This support is gratefully acknowledged.

References

Clarke, John L (2003). *Structural design of polymer composites: Eurocomp design code and background document*. CRC Press.

González, Sara Ferreño and Vicente Diaz-Casas (2016). "Present and Future of Floating Offshore Wind". In: *Floating Offshore Wind Farms*. Ed. by Laura Castro-Santos and Vicente Diaz-Casas. Cham: Springer International Publishing, pp. 1–22. ISBN: 978-3-319-27972-5. DOI: 10.1007/978-3-319-27972-5_1. URL: https://doi.org/10.1007/978-3-319-27972-5_1.

Jurado Granados, Joel (2021). "Desarrollo e implementación de una formulación utilizando la teoria de mezclas serie/paralelo para la modelización de estructuras navales de materiales compuestos sometidas bajo cargas cıclicas". In.

Manzano-Agugliaro, Francisco et al. (Jan. 2020). "Wind Turbines Offshore Foundations and Connections to Grid". In: *Inventions 2020, Vol. 5, Page 8* 5 (1), p. 8. ISSN: 2411-5134. DOI: 10.3390/INVENTIONS5010008. URL: https://www.mdpi.com/2411-5134/5/1/8/htm%20https://www.mdpi.com/2411-5134/5/1/8.

Marshall, Peter William (2013). *Design of welded tubular connections: basis and use of AWS code provisions*. Vol. 37. Elsevier.

Mehmanparast, Ali, Saeid Lotfian, and Sukumara Pillai Vipin (2020). "A review of challenges and opportunities associated with bolted flange connections in the offshore wind industry". In: *Metals* 10.6, p. 732.

Oh, Ki Yong et al. (May 2018). "A review of foundations of offshore wind energy convertors: Current status and future perspectives". In: *Renewable and Sustainable Energy Reviews* 88, pp. 16–36. ISSN: 1364-0321. DOI: 10.1016/J.RSER.2018.02.005.